COMPDYN 2015
5th ECCOMAS Thematic Conference on
Computational Methods in Structural Dynamics and Earthquake Engineering
M. Papadrakakis, V. Papadopoulos, V. Plevris (eds.)
Crete Island, Greece, 25–27 May 2015

TIME DOMAIN SIMULATION OF VORTEX-INDUCED VIBRATION OF A CURVED BEAM USING A WAKE OSCILLATOR MODEL

Y. Qu[1], **A.V. Metrikine**[1]

[1] Delft University of Technology
Faculty of Civil Engineering & Geosciences
Stevinweg 1, 2628CM Delft, the Netherlands
e-mail: Y. Qu@tudelft.nl，A.Metrikine@tudelft.nl

Keywords: Time Domain, Vortex-induced Vibration, Wake Oscillator, Flexible Cylinder, Curved Beam.

Abstract. *A general model capable of simulating the vortex-induced vibration of a flexible curved cylinder is presented. The 3-D motion of the cylinder is modeled using a curved Euler-Bernoulli beam, which accounts for bending, extensibility and geometrical nonlinearity. The finite element method is used to solve the beam equation. The hydrodynamic forces are modelled with the help of the van der Pol wake oscillators attached to the nodes of the FE model of the beam. Such phenomenological oscillators are conventionally used for the prediction of vortex-induced vibration of rigid cylinders subjected to cross flow perpendicular to their axis. In order to cope with the curvature of the beam, a local reference frame is introduced and the tangential component of the flow velocity is neglected. Comparison is performed of the predictions of the proposed model with experimental observations of the vortex-induced vibration of a curved cable available in the literature. The comparison showed that the proposed model can reproduce some features observed in the experiment, such as the location of power-in region and the travelling wave.*

1 INTRODUCTION

In offshore engineering applications, slender structures such as risers, cables and pipelines are widely used. These types of structures usually have very large aspect ratio (L/D) and have to be considered as flexible. When exposed to marine currents, these slender structures undergo vortex-induced vibrations (VIV) due to the space-time varying hydrodynamics associated with vortex shedding. The prediction of VIV is one of the key issues in the analysis and design of offshore slender structures because these vibrations result in significant fatigue damage.

Although VIV of a short rigid cylinder has been well documented in many reviews [1, 2, 3], the features of VIV of long slender structures have not been fully understood. A review of the recent studies on the VIV of long slender cylinders can be found in [4].

In the prediction of VIV of a short rigid cylinder, nonlinear wake oscillator models have been widely used in recent years and gained popularity due to the low computational effort and acceptable accuracy. In [5], a classical van der Pol oscillator is used to model the near wake dynamics and the effects of several types of linear coupling terms (displacement, velocity and acceleration) modelling the fluid-structure interaction are investigated. It was found in [5] that the acceleration coupling is most appropriate for the modelling of most of the features of VIV. This van der Pol oscillator model was further improved by properly including the effect of stall term dropping the assumption of a small angle of attack [6].

Several papers can be found in the literature, which employ the wake oscillator models for the prediction of VIV of straight flexible cylinders exposed to a normal cross flow. In contrast, the VIV of curved cylinders has not been widely addressed. In all known to the authors works on this matter, strong simplifications have been made regarding either the flow direction [7, 8] or the motion of the cylinder [9].

The main novelty of this paper lies in the improved model of the cylinder-wake interaction, which includes the geometric nonlinearity of the structure and a projection of the initially inclined to the cylinder axis flow direction.

2 MODEL DISCRIPTION

2.1 Nonlinear structural model

In theoretical studies of VIV of slender cylinders, the latter are usually modelled by straight tensioned beams or cables whose equations of motion (excluding the hydrodynamic forces) are assumed to be linear. However, in practical applications many slender structures, such as catenary risers, pipelines during the laying process and mooring cables have a curved shape. So a general Euler-Bernoulli beam model valid for both curved and straight cylindrical structures is used here. It accounts for bending, extensibility and geometrical nonlinearity. The description of the beam position is based on the differential geometry of 3D curves [10] where the arbitrary point on the beam axis can be described by a position vector $\mathbf{r}$:

$$\mathbf{r}(s,t)=\begin{bmatrix} x(s,t) \\ y(s,t) \\ z(s,t) \end{bmatrix}, \tag{1}$$

where s is the Eulerian coordinate measured along the stretched beam and t is the time. Let us introduce the tangential unit vector $\mathbf{t}=\partial\mathbf{r}/\partial s$, the principle normal unit vector $\mathbf{n}$ and the binormal unit vector $\mathbf{b}$, such that $\mathbf{b}=\mathbf{t}\times\mathbf{n}$, $\mathbf{n}=\mathbf{b}\times\mathbf{t}$ and $\mathbf{t}=\mathbf{n}\times\mathbf{b}$. The curvature vector of the beam is $\mathbf{k}=\partial\mathbf{t}/\partial s=\partial^2\mathbf{r}/\partial s^2$, and the axial strain of the beam is $\varepsilon=|\partial\mathbf{r}/\partial p|-1$, where p is the Lagrangian co-

ordinate measured along the unstretched beam. It should be noted that the torsion of the beam is ignored here. For the convenience of writing, the following notation will be used to represent the partial derivative with respect to s: $\mathbf{r}_{,s}=\partial\mathbf{r}/\partial s$.

The weak form of the equations of motion of the beam is derived from the Lagrange-D'Alembert equation:

$$\delta W_E - \delta W_S = \delta W_I, \tag{2}$$

where δW_E denotes the virtual work of the external forces, δW_S is the virtual work done by the internal forces and δW_I is the virtual work of the inertial forces. The elastic internal forces are split into two parts, namely a part due to bending based on the curvature of the deformed beam, and a part due to axial strain. The virtual work done by the axial force is given as

$$\delta W_A = \int_0^l EA\varepsilon\mathbf{r}_{,s}\bullet\delta\mathbf{r}_{,s}ds, \tag{3}$$

while the virtual work due to bending reads

$$\delta W_B = \int_0^l \left(EI\mathbf{r}_{,ss}\bullet\delta\mathbf{r}_{,ss} - EI\kappa^2\mathbf{r}_{,s}\bullet\delta\mathbf{r}_{,s} \right)ds, \tag{4}$$

where EI is the bending stiffness, EA is the axial stiffness and l is the length of the beam in deformed configuration. Then the total virtual work of internal forces can be written as

$$\delta W_S = \int_0^l \left(EI\mathbf{r}_{,ss}\bullet\delta\mathbf{r}_{,ss} - EI\kappa^2\mathbf{r}_{,s}\bullet\delta\mathbf{r}_{,s} + EA\varepsilon\mathbf{r}_{,s}\bullet\delta\mathbf{r}_{,s} \right)ds. \tag{5}$$

For the virtual work of the inertial forces, the rotational inertia is ignored and only the inertia due to the linear acceleration is considered. Thus

$$\delta W_I = \int_0^l m\ddot{\mathbf{r}}\delta\mathbf{r}ds \tag{6}$$

where m is the mass of the beam per unit length in the deformed configuration. When this model is applied in the simulation of the VIV, m includes the ideal added mass $m_a=1/4\,\pi C_a\rho D^2$, in which ρ denotes the density of the fluid, D is the outer diameter of the cylinder and C_a is the added mass coefficient which is assumed to be equal to one in this paper.

As the formulas presented above are derived in the frame of the Eulerian description, they need to be transformed to the Lagrangian description where the original length of the beam L is already known. The relations used for the transformation are

$$\mathbf{r}_{,s} = \frac{1}{\left|\mathbf{r}_{,p}\right|}\mathbf{r}_{,p},\ \mathbf{r}_{,ss} = \frac{1}{\left|\mathbf{r}_{,p}\right|^3}\left(\left|\mathbf{r}_{,p}\right|\mathbf{r}_{,pp} - \frac{\mathbf{r}_{,p}\bullet\mathbf{r}_{,pp}}{\left|\mathbf{r}_{,p}\right|}\mathbf{r}_{,p} \right) \text{ and } ds = \left|\mathbf{r}_{,p}\right|dp. \tag{7}$$

Applying these relations to Eq. (4) and (5), we obtain

$$\delta W_A = \int_0^L EA\frac{\left(\left|\mathbf{r}_{,p}\right|-1\right)}{\left|\mathbf{r}_{,p}\right|}\mathbf{r}_{,p}\bullet\delta\mathbf{r}_{,p}dp \tag{8}$$

and

$$\delta W_B = \int_0^L EI \frac{1}{\left|\mathbf{r}_{,p}\right|^5}\left(\left(\left|\mathbf{r}_{,p}\right|^2 \mathbf{r}_{,pp} - \left(\mathbf{r}_{,p} \bullet \mathbf{r}_{,pp}\right)\mathbf{r}_{,p}\right) \bullet \delta \mathbf{r}_{,pp} + \left(\left(\frac{\mathbf{r}_{,p} \bullet \mathbf{r}_{,pp}}{\left|\mathbf{r}_{,p}\right|}\right)^2 \mathbf{r}_{,p} - \left(\mathbf{r}_{,p} \bullet \mathbf{r}_{,pp}\right)\mathbf{r}_{,pp} + \kappa^2 \left|\mathbf{r}_{,p}\right|^4 \mathbf{r}_{,p}\right) \bullet \delta \mathbf{r}_{,p}\right) dp, \tag{9}$$

where

$$\kappa = \left|\mathbf{r}_{,ss}\right| == \frac{1}{\left|\mathbf{r}_{,p}\right|^3}\left|\mathbf{r}_{,pp} \times \mathbf{r}_{,p}\right|. \tag{10}$$

A two nodes beam element, the same as the one described in [11], is used in this paper. The vector of nodal coordinates of the element consists of 12 degrees of freedom

$$\begin{aligned} \mathbf{e}^T = \big[& x(0) \quad y(0) \quad z(0) \quad x_{,p}(0) \quad y_{,p}(0) \quad z_{,p}(0) \\ & x(L_0) \quad y(L_0) \quad z(L_0) \quad x_{,p}(L_0) \quad y_{,p}(L_0) \quad z_{,p}(L_0) \big], \end{aligned} \tag{11}$$

where L_0 is the length of the beam element. Based on that, the global position vector of an arbitrary point, originally placed at p of the undeformed beam axis, in the deformed configuration can be interpolated in terms of the nodal coordinates and the element shape function as

$$\mathbf{r} = \begin{bmatrix} x \\ y \\ z \end{bmatrix} = S\mathbf{e}. \tag{12}$$

A cubic polynomial shape function is employed to describe each components of the position vector. Thus, the global shape function S can be written as

$$S = [S_1\mathbf{I} \quad S_2\mathbf{I} \quad S_3\mathbf{I} \quad S_4\mathbf{I}], \tag{13}$$

where $\mathbf{I}$ is the 3×3 unit matrix and the function $S_i = S_i(p)$ are given by

$$\begin{aligned} & S_1 = 2\left(\frac{p}{L}\right)^3 - 3\left(\frac{p}{L}\right)^2 + 1, S_2 = L\left(\frac{p}{L}\right)^3 - 2L\left(\frac{p}{L}\right)^2 + p, \\ & S_3 = 3\left(\frac{p}{L}\right)^2 - 2\left(\frac{p}{L}\right)^3, S_4 = L\left(\left(\frac{p}{L}\right)^3 - \left(\frac{p}{L}\right)^2\right). \end{aligned} \tag{14}$$

2.2 Wake oscillator model

In this study, a van der Pol wake oscillator model proposed in [6] is used to compute the hydrodynamic forces due to vortex shedding. In order to introduce the model, let us consider a case where cylinder is rigid and flow is perpendicular to its axis. By assuming that the flow around the cylinder is two-dimensional (uniform along the cylinder axis), the interaction between the cylinder and the flow can be simplified as shown in Fig. 1. The total vortex force acting on per unit length of the cylinder is decomposed into a drag part F_{VD} and a lift part F_{VL}, where the drag and the lift are defined as, respectively, being in-line with and perpendicular to

U, the latter being the total flow velocity relative to the moving cylinder. The lift force $F_{VL}(s,t)$ is expressed through the wake variable $q(s,t)$ as

$$F_{VL} = \frac{1}{2}\rho D U^2 C_{VL}, \qquad C_{VL} = \frac{C_L}{2} q, \tag{15}$$

where C_L is the lift coefficient measured for a stationary cylinder. Furthermore, the inertial coupling is assumed between the wake oscillator and the structure:

$$\frac{d^2 q}{dt^2} + \varepsilon \omega_s \left(q^2 - 1\right)\frac{dq}{dt} + \omega_s^2 q = \frac{A}{D}\frac{d^2 Y}{dt^2} \tag{16}$$

where ω_s is the Strouhal frequency, whereas A and ε are tuning parameters.

The drag force $F_{VD}(s,t)$ is defined as

$$F_{VD} = \frac{1}{2}\rho D U^2 C_{VD}, \qquad C_{VD} = C_D, \tag{17}$$

where C_D is the drag coefficient measured for a stationary cylinder.

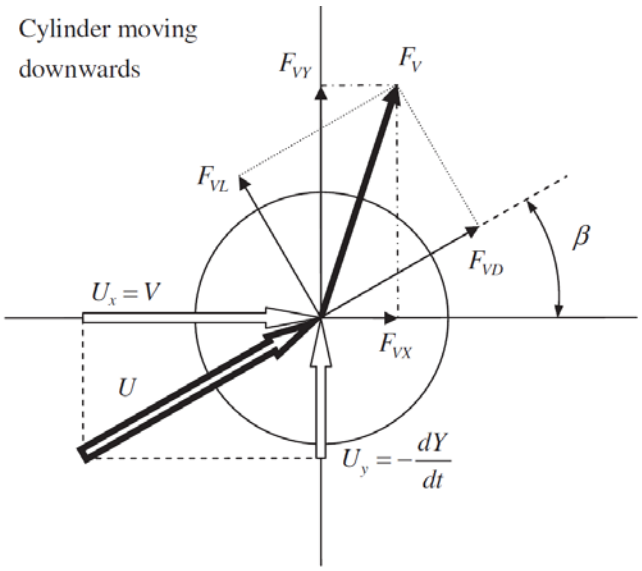

Figure 1: Decomposition of the vortex fluid force in drag, lift, X and Y direction [6].

The force acting on the cylinder in the Y (vertical) direction due to the vortex shedding is given as

$$F_{VY} = \frac{1}{2}\rho D V^2 C_{VY} = \frac{1}{2}\rho D \sqrt{V^2 + \left(\frac{dY}{dt}\right)^2}\left(C_{VL} - C_{VD}\left(\frac{dY}{dt}\right)\right). \tag{18}$$

In order to gain insight into the conditions under which the VIV may occur, let us assume that the cylinder is forced to vibrate in the cross-flow direction harmonically with an amplitude y and a frequency ω_c:

$$Y(t) = y \sin(\omega_c t). \tag{19}$$

Substituting Eq.(19) into Eq. (15) and then using the following dimensionless parameters

$$\tau = \omega_s t,\ \Omega_c = \omega_c / \omega_s,\ \hat{y} = y/D, \tag{20}$$

we obtain

$$\frac{d^2 q}{d\tau^2} + \varepsilon\left(q^2 - 1\right)\frac{dq}{d\tau} + q = -A\Omega_c \hat{y}\sin\left(\Omega_c \tau\right). \tag{21}$$

Applying the same procedure to Eq. (18), the following expression can be obtained for C_{VY}:

$$C_{VY} = \left(-2\pi \mathrm{St}\hat{y}\Omega_c \cos\left(\Omega_c \tau\right) C_{VD} + C_{VL}\right)\sqrt{1 + 4\pi^2 \mathrm{St}^2 \Omega_c^2 \cos^2\left(\Omega_c \tau\right)} \tag{22}$$

According to the harmonic balance method and accounting for the contribution of the fundamental frequency only, the solution to Eq. (21) is sought for in the form $q = q_0 \sin\left(\Omega_c t + \varphi\right)$. Substituting the latter expression in Eq. (22) and considering only the main harmonic contribution of the nonlinearities, collection of multipliers of $\sin\left(\Omega_c t\right)$ and $\cos\left(\Omega_c t\right)$ yields two algebraic equations with two unknowns q_0 and φ. Then the component of C_{VY} that in phase with the velocity of the cylinder can be approximated as

$$C_{yv} \approx \left(-2\pi \mathrm{St}\hat{y}\Omega_c C_{VD} + \frac{1}{2} C_L q_0 \sin\left(\varphi\right)\right)\sqrt{1 + 4\pi^2 \mathrm{St}^2 \Omega_c^2} \tag{23}$$

It is the sign of C_{yv} in Eq. (23) that implies whether the flow provides the cylinder with the energy or extracts it from the moving cylinder. If C_{yv} is positive, the flow increases the energy of the cylinder while otherwise the energy of the vibration of the cylinder will be reduced due to interaction with the flow. As can be seen from Eqs. (21) and (23), if tuning parameters A and ε are fixed, the sign of C_{vy} depends on the dimensionless amplitude $\hat{y}$ and dimensionless frequency Ω_c. In Fig 2 the density plots of C_{vy} are shown in the plane of the reduced velocity $V_c = 1/\mathrm{St}/\Omega_c$ and the normalized amplitude $\hat{y} = y/D$ for two sets of the tuning parameters. For both cases, the following figures for the other parameters are used: St=0.17, C_{VD}=1.2, and C_L=0.3842.

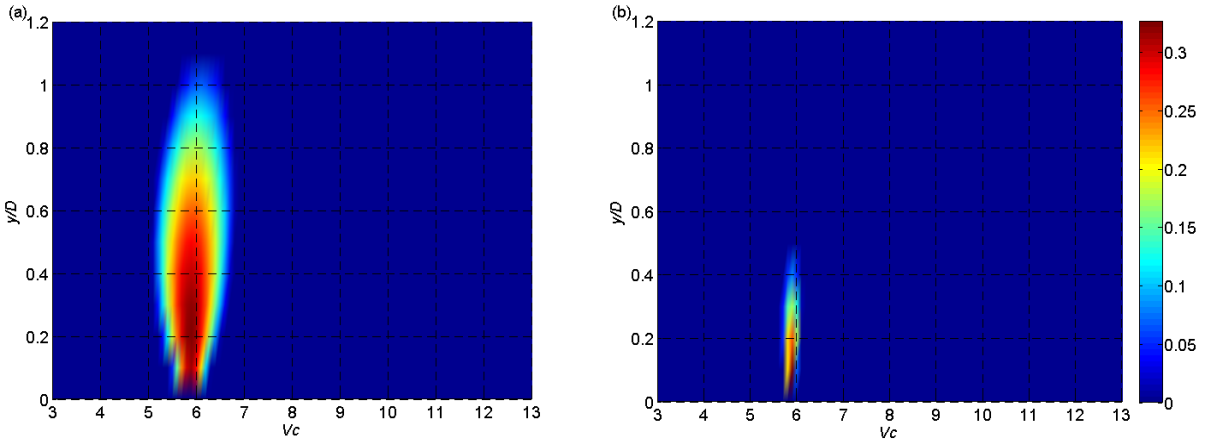

Figure 2: Force coefficient C_{yv} in phase with the velocity of the cylinder: (a) A=4, ε=0.05, (b) A=1, ε=0.1.

As can be seen from Fig 2, the power-in range can depends significantly on the tuning parameters. In Fig 2a, the power-in region is located approximately between reduced velocity 5 and 7, and the maximum amplitude in this range is about 1D. In Fig 2b, due to the small pa-

rameter A, the power-in range is extremely narrow and is localized around the reduced velocity of 6. The maximum amplitude in the power-in range in the latter case is less than 0.5D.

2.3 Coupled system

As mentioned before the wake oscillator model described above has been developed for rigid cylinders subject to the normal cross flow. However, for the VIV of long flexible cylinder, the attack angle and relative to the flow velocity of the cylinder depend on the position along the cylinder. In this paper, by assuming that the Independence Principle is valid and the vortex shedding is correlated within certain length of the cylinder, the wake oscillators are attached to the nodes of beam elements where local frames are used so the wake oscillator described before is applicable.

Using the local frame described by the tangent, principal normal and binormal unit vectors, the 2-D vortex shedding process is assumed to happen in the plane (i.e., **b**-**n** plane) that is perpendicular to the orientation of the beam, see Fig 3.

The absolute normal flow velocity and the relative normal flow velocity are given by

$$\begin{aligned} \mathbf{V}_N &= \mathbf{V} - \left(\mathbf{V}\bullet\mathbf{t}_s\right)\mathbf{t}_s, \\ \mathbf{U}_N &= \mathbf{U} - \left(\mathbf{U}\bullet\mathbf{t}\right)\mathbf{t}, \end{aligned} \tag{24}$$

where $\mathbf{V}$ is the flow velocity in the earth-bound reference frame, $\mathbf{U}$ is the relative flow velocity and $\mathbf{t}_s$ is the unit tangent vector measured under the initial static configuration due to the mean in-line forces.

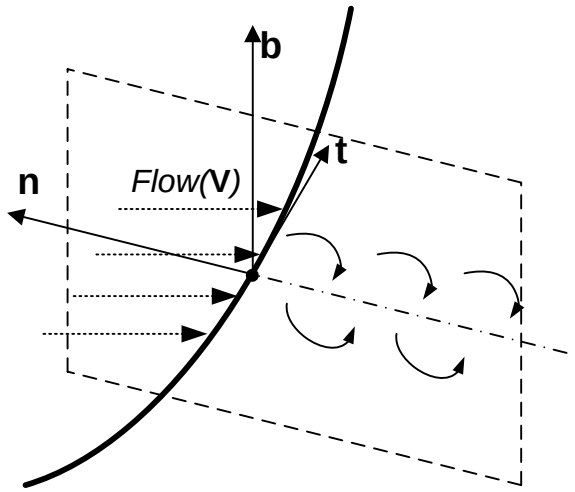

Figure 3: Local vortex shedding for a spatial curved cylinder.

The lift and drag forces are defined as

$$\mathbf{F_L} = \frac{1}{2}\rho DL\frac{C_L}{2}q\left|\mathbf{U_N}\right|^2\mathbf{D_L}, \tag{25}$$

$$\mathbf{F_D} = \frac{1}{2}\rho DLC_D\left|\mathbf{U_N}\right|\mathbf{U_N}, \tag{26}$$

where $\mathbf{D_L}$ is the direction of the lift force:

$$\mathbf{D}_{\mathbf{L}} = \frac{\mathbf{U}_{\mathbf{N}} \times \mathbf{t}}{\left|\mathbf{U}_{\mathbf{N}} \times \mathbf{t}\right|}. \tag{27}$$

The coupling term in the wake oscillator equation is also changed accordingly:

$$\ddot{q} + \varepsilon\omega_s \left(q^2 - 1\right)\dot{q} + \omega_s^2 q = \frac{A}{D}\ddot{\mathbf{r}} \bullet \mathbf{D}_{\mathbf{a}}, \tag{28}$$

where

$$\mathbf{D}_{\mathbf{a}} = \frac{\mathbf{V}_{\mathbf{N}} \times \mathbf{t}_s}{\left|\mathbf{V}_{\mathbf{N}} \times \mathbf{t}_s\right|}. \tag{29}$$

One of the major drawbacks of the approach adopted in this paper is that the Independence Principle is not applicable for large angles between the flow and the cylinder axis. Experiments showed that there is a critical angle above which the relatively wide plateau of the large amplitude oscillations observed in the case of small attack angles disappears and, instead, large-amplitude oscillations occur in a very narrow range of normalized reduced velocities [12]. This means that the parameters of the wake oscillator model should be dependent on the local inclination of the cylinder. For convenience, in this paper only two sets of tuning parameters are used. One set corresponds to the inclination smaller than the critical angle, and the other one is used when inclination is bigger than the critical angle.

3 COMPARISON WITH EXPERIMENTAL RESULTS

In this section, results of a case study are presented and compared with those of a large-scale field test. The objective is to check if experimentally observed results can be reproduced by the model introduced in the previous sections.

A series of field tests were conducted by MIT and the Deepstar Consortium in and near the Gulf Stream in 2004 and 2006. The specific test selected for comparison in this paper is described in [13]. In the tests, a fiber glass composite pipe of 152.4 meters long and 3.63 cm in outer diameter was towed in Gulf Stream with a railroad wheel attached to the tip of the pipe to provide tension. A diagram of the test configuration is shown in Fig. 4. The properties of the pipe are summarized in Table 1.

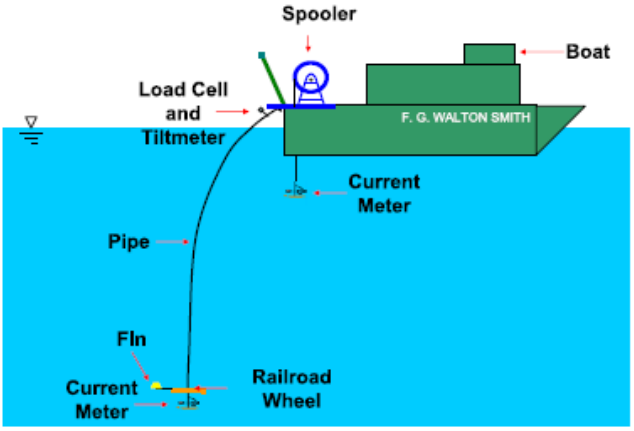

Figure 4: Set-up of the Gulf Steam experiments 2006 [14].

When towed in water, due to the tension applied at the tip and the drag forces acting on the pipe, it will assume a curved shape. This shape defines the angle of attack at various positions

along the pipe. In [13], no information about the pipe shape is given. Only the distribution of the normal velocity of the current relative to the deformed shape is given. In order to get the shape of the pipe, static analysis of the pipe under uniform current is carried out. The drag coefficients were iterated until the calculated and the given in [13] normal current profiles matched each other. Since the wake oscillator model underestimates the amplification of drag forces due to VIV, extra in-line forces were applied during dynamic analysis to maintain the shape.

Parameters	Value
Inner Diameter	0.0249 m
Outer Diameter	0.0363 m
EI	613 Nm^2
EA	3.322e6 N
Weight in sea water	0.1972 kg/m
Weight in air	1.2682 kg/m
Effective Tension	3225 N
Length	152.4 m

Table 1: Gulf Stream 2006 pipe properties.

In view of many uncertainties involved in the experiment, the focus of this paper is placed on the qualitative reproduction of the test results. According to [14, 15], the power-in region is set to belong in the reduced velocity interval from 5 to 7, and the critical angle of inclination is set to 45 degrees. The adopted parameters of the wake oscillator model are given in Table 2.

Parameters	Value
St	0.17
A	4 ($\theta < 45$) 1 ($\theta > 45$)
epsilon	0.05 ($\theta < 45$) 0.1 ($\theta > 45$)

Table 2: Parameters of wake oscillator.

Fig 5 shows the time evolution of the cable response as resulted from both the test and the simulation. The time period from 20 to 30 seconds of the simulation is chosen. Similar to the test, a strong presence of traveling waves along the cable is observed. The dominant waves are generated from the power-in region at the bottom of the cable and then propagate upwards. There are also differences between the simulation results and test data. The most obvious one is that the simulation also predicts waves with lower frequency generated at the top of the cable which then propagate downwards. Intermittent standing waves are observed in the region where the waves travelling upwards and downwards interact. Another difference is that in experiments standing waves are observed at the bottom of the cable due to the reflective boundary condition at the tip. The simulations do not show such a phenomenon. The first difference may be attributed to additional factors that could influence the test results. For example, the VIV generated at the top of the cable might be significantly suppressed by the waves or the motions of the boat.

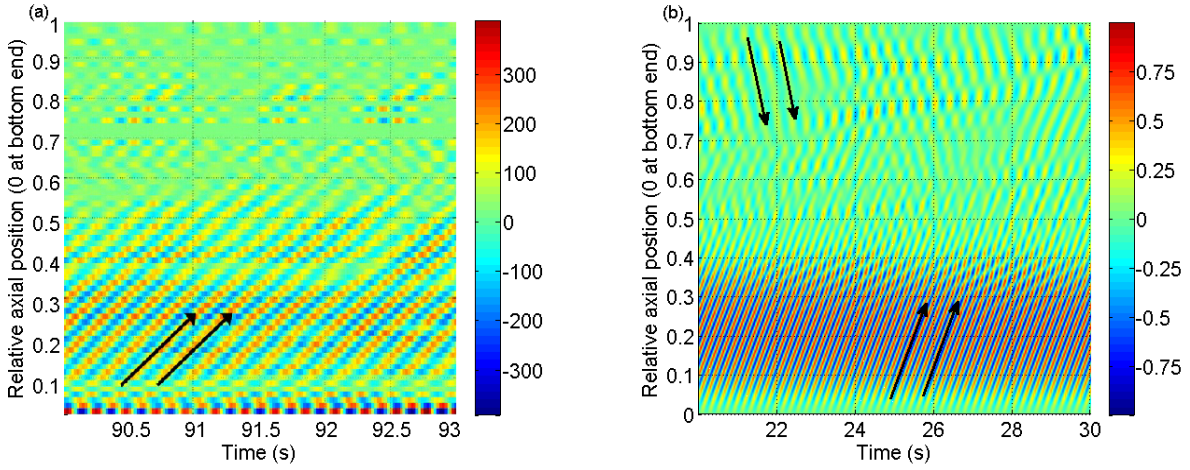

Figure 5: Evolution of the cable response in time and space: (a) fundamental harmonic strain observed in the test; (b) dimensionless cross-flow displacement obtained in simulations.

In order to find a reason for the absence of the standing waves near the tip in the simulations and to understand whether the response of the cable is dependent on the initial conditions, several simulations are conducted with varying initial conditions.

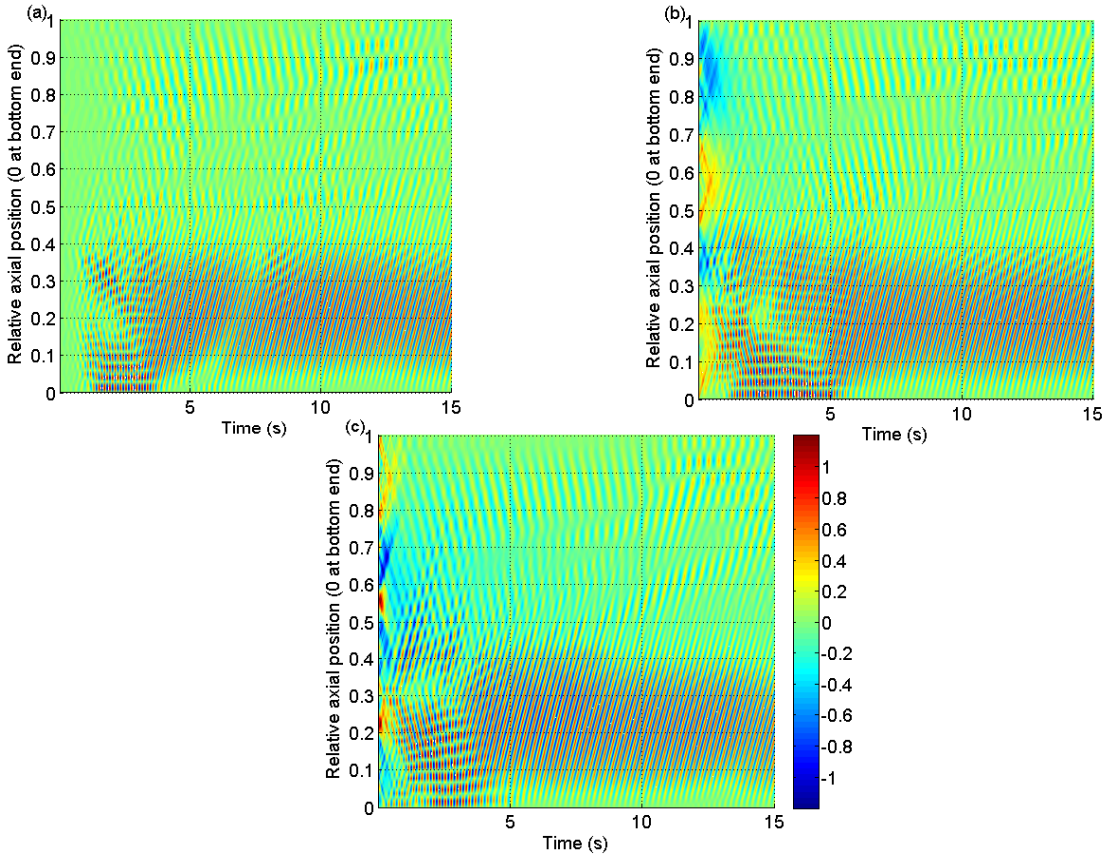

Figure 6: Time evolution of the cross-flow dimensionless displacement in three simulations with different initial conditions.

Fig. 6 shows results of three simulations with different initial conditions. It can be seen that initial conditions do not have apparent influence on pattern of the cross-flow response. For all three cases, the dominant waves are generated at the tip of the pipe and propagate upwards. It

is also noticeable that, in the beginnings of all three simulations, standing waves occur near the tip. However, these standing waves seem to be unstable and are replaced by travelling waves within a few seconds.

Fig. 7 gives a zoom in on the time evolution of the fluctuating lift force (in terms of the wake variable q) acting on lower half of the cable. Results of the same simulation are presented as used for plotting Fig. 6b. Fig. 7 shows that the excitation force is also in the form of a travelling wave which is expectable. However, the evolution of the pattern of the lift force in time is quite interesting. First, a standing wave seems to be present, which is later transferred into a travelling wave. An additional investigation is needed in order to conclude whether such an evolution is generic or it occurs only for specific combinations of the system parameters.

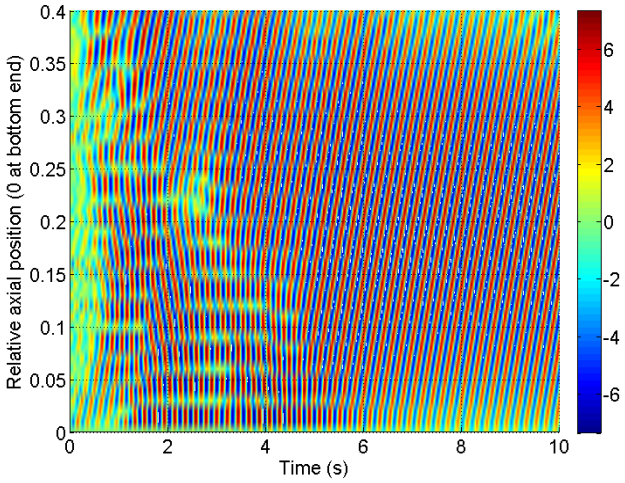

Figure 7: Time evolution of wake variable q .

4 CONCLUSIONS

A model capable of simulating the vortex-induced vibrations of a curved flexible cylinder has been developed. The cylinder model is based on the Euler-Bernoulli beam theory and accounts for bending, extensibility and geometrical nonlinearity. The spatial configuration of the cylinder is described by a position vector, and the 3D motion of the cylinder is solved for using the finite element method. Wake oscillators are attached to the nodes of the structural model to mimic the fluctuating lift and drag forces due to the hydrodynamic interaction of the cylinder with the flow.

A comparison with results of a large-scale test has shown that the developed model can predict main features of the VIV of a long curved cable. The presence of travelling wave that has been observed in the test has been successfully reproduced and the power-in region has been located correctly. However, the model failed to capture the standing waves observed near the tip of the cable in the test. The standing waves generated near the tip at the beginning of simulations seem to be unstable and are gradually replaced by travelling waves within a few seconds. Simulations have also shown that the initial conditions do not have perceptible influence on the steady-state response of the cable.

REFERENCES

[1] T. Sarpkaya, A critical review of the intrinsic nature of vortex-induced vibrations. *Journal of Fluids and Structures*, 19, 389-447, 2004.

[2] R.D. Gabbai, H. Benaroya, An overview of modelling and experiments of vortex-induced vibration of circular cylinder. *Journal of Sound and Vibration*, 282, 575-616, 2005.

[3] P.W. Bearman, Circular cylinder wakes and vortex-induced vibrations. *Journal of Fluid Mechanics*, 27, 648-658, 2011.

[4] X. Wu, F. Ge, Y. Hong, A review of recent studies on vortex-induced vibrations of long slender cylinders. *Journal of Fluids and Structures*, 28, 292-308, 2012.

[5] M.L Facchinetti, E. de Langre, F. Biolley, Coupling of structure and wake oscillators in vortex-induced vibrations. *Journal of Fluids and Structures*, 19 (2), 123-140, 2004.

[6] R.H.M. Ogink, A.V. Metrikine, A wake Osicllator with Frequency Dependent Coupling for the Modelling of Vortex-Induced Vibration. *Journal of Sound and Vibration*, 329, 5452-5473, 2010.

[7] N. Srinil, M. Wiercigroch, P. O'Brien, Reduced-order modelling of vortex-induced vibration of catenary riser. *Ocean Engineering*, 36, 1404-1414, 2009.

[8] N. Srinil, Multi-mode interactions in vortex-induced vibrations of flexible curved/straight structures with geometric nonlinearities. *Journal of Fluids and Structures*, 26, 1098-1122, 2010.

[9] W. Qin, Z. Kang, R. Song, L. Sun, Y. Wu, A New Wake Oscillator Modeling of Vortex-Induced Vibration of SCR in Two Degrees of Freedom. *23rd International Offshore and Polar Engineering (ISOPE 2013),* Anchorage, Alaska, USA, June 30-July 5, 2013.

[10] B. O'Neil, Elementary Differential Geometry, 2nd Edition, San Diego, 2006.

[11] J. Gerstmary, A.A. Shabana, Analysis of Thin Beams and Cables Using the Absolute Nodal Co-ordinate Formulation. *Nonlinear Dynmaics*, 45, 109-130, 2006.

[12] A. Jain, Y. Modarres-Sadeghi, Vortex-induced vibration of a flexibly-mounted inclined cylinder. *Journal of Fluids and Structures*, 43, 28-40, 2013.

[13] J. Kim Vandiver, V. Jaiswal, V. Jhingran, Insights on vortex-induced, traveling waves on long risers. *Journal of Fluids and Structures*, 25, 641-653, 2009.

[14] S.B. Swithenbank, J. Kim Vandiver, Identifying the power-in region for vortex-induced vibrations of long flexible cylinders. *26th International conference on Offshore Mechanics and Arctic Engineering (OMAE 2007),* San Diego, California, USA, June 10-15, 2007.

[15] V. Jaiswal, A. Sheshadri, J. Kim Vandiver, Modelling Traveling Waves using Mode Superposition. *29th International conference on Ocean, Offshore and Arctic Engineering (OMAE 2010),* Shanghai, China, June 6-11, 2010.